Solid Earth Discuss., doi:10.5194/se-2016-38, 2016
Manuscript under review for journal Solid Earth
Published: 16 March 2016
© Author(s) 2016. CC-BY 3.0 License.



Solid Earth Discussions
Open Access
EGU

Porosity and permeability determinations of organic rich Posidonia shales based on 3D analyses by FIB-SEM microscopy

Georg H. Grathoff[1] , Markus Peltz[1], Frieder Enzmann[2] & Stephan Kaufhold[3]

[1]Department of Geography and Geology, EMA University of Greifswald, Greifswald, 17489, Germany
[2]Institute for Geosciences, J. Gutenberg University Mainz, Mainz, 55128,Germany
[3]Bundesanstalt für Geowissenschaften und Rohstoffe, Hannover, 30655, Germany

Correspondence to: Georg H. Grathoff (grathoff@uni-greifswald.de)

Abstract. The goal of this study is to better understand the porosity and permeability in shales to improve modelling fluid and gas flow related to shale diagenesis. Two samples (WIC and HAD) were investigated, both Mid Jurassic Posidonia organic rich shales from central Germany of different maturity (WIC R_0 0.53% and HAD R_0 1.45%). The method for image collection was Focused Ion Beam (FIB) microscopy coupled with Scanning Electron Microscopy (SEM). For image and data analysis Avizo and GeoDict was used. Porosity was calculated from segmented 3D FIB based images and permeability was simulated by a Navier Stokes-Brinkman solver in the segmented images.

Results show that the quantity and distribution of pore clusters and pores ($\geq$ 40nm) are similar. The largest pores are located within carbonates and clay minerals, whereas the smallest pores are within the matured organic matter. Orientation of the pores calculated as pore paths showed minor directional differences between the samples, possibly due to maturation. Both samples have no axis connectivity of pore clusters in the x, y, and z direction on the scale of 10 to 20 of micrometer, but do show connectivity on the micrometer scale. The volume of organic matter in the studied volume is representative of the TOC in the samples. Organic matter does show axis connectivity in the x, y, and z direction. With increasing maturity the porosity in organic matter increases from close to 0 to more than 5 %. These pores are small and in the large organic particles have little connection to the mineral matrix. Continuous pore size distributions are compared with Mercury Intrusion Porosimetry (MIP) data. Minor differences are caused by resolution limits of the FIB-SEM and by the development of small pores during the maturation of the organic matter. Calculations show no permeability when only considering visible pores due to the lack of axis connectivity. Adding the organics with a background permeability of 1e-22 m^2 to the calculations, the total permeability increased by one to two orders of magnitude depending on the direction of flow boundary conditions. Our results compare well with experimental data from the literature suggesting that upscaling may be possible in the future.

1 Introduction

The investigated organic rich Posidonia shales are Mid-Jurassic in age from the Hils Syncline of Northwestern Germany. The investigated sample come from a larger sample set studied at the BGR as part of their NIKO project (Kaufhold et al.

Solid Earth Discuss., doi:10.5194/se-2016-38, 2016
Manuscript under review for journal Solid Earth
Published: 16 March 2016
© Author(s) 2016. CC-BY 3.0 License.



2015). Kaufhold et al. (2015) compared the direct methods of Focussed Ion Beam – Scanning Electron Microscopy (FIB-SEM) and Micro Computer Tomography (µCT) with the indirect methods of Mercury Intrusion Porosimetry (MIP) and gas adsorption (N_2 and CO_2) and found that 80 % of the porosity was below 30 nm, which can be barely detected by FIB-SEM and was not recognizable by µCT. For our study we took a more detailed look at 2 of the samples: 1 Wickensen (WIC) with the lowest vitrinite reflectance (R_0) of 0.53 % representing the start of oil generation and 2. Haddessen (HAD) with a vitrinite reflectance of 1.45 % representing the gas window. For further details about the samples and the geology see Schlosser et al. (2015) and references there in.

The porosity and permeability of organic-rich shales have become of increased interest due to the growing exploitation of unconventional hydrocarbons. Goal of this study is to better understand the porosity, permeability and pore network development in shales using FIB-SEM to improve our understanding of fluid and gas flow related to shale diagenetic history. Pores typically reflect depositional and diagenetic processes that the shale has undergone. These processes include sediment transport, deposition, compaction, cementation and dissolution, mainly of carbonates and silicates, organic maturation and clay mineral diagenesis (e.g. Loucks et al. (2012)). All these processes effect both the porosity, permeability, and the pore network. Therefore it is important to separate different types of pores due to their different origin and their different behavior after deposition. Pores are three dimensional objects that can be characterized by their size, location, and network (e.g. Schieber (2011) & Loucks et al. (2012))

The pore sizes are often classified according to the classification of International Union of Pure and Applied Chemistry (IUPAC) as developed by Rouquerol et al. (1994). They divide the pores into micropores (< 2nm pore width), mesopores (2-50 nm pore width), and macropores (>50 nm pore width). Recently Chalmers et al. (2012) suggested to use the IUPAC pore size definition to divide the pore sizes in shales. The other option of determining the actual size of each connected pore system (= pore clusters) is to measure the physical area (for 2D) or volume (3D) of the photomicrograph. The total pore space is the same from both methods. The difference is that individual pore clusters are significantly larger than the continuous pore size distribution.

Pores of the same size can occur in various locations: inside different minerals (e.g. phyllosilicates and other silicates, carbonates, sulfides) and organics as well as between mineral grains. Based on petrological observations Schieber (2011) divides pores up into Framework Pores, which are pores that primary between individual grains (i.e. phyllosilicates, carbonates), Intrapores, which are pores within grains, Solvopores, which are secondary pores formed from dissolution, Macerapores, which are pores associated with organic matter and its ripening, and Desipores, which are artifacts due to the shrinking, desiccation caused by drying of clay minerals and organics. He also reported that the detrital clay minerals appear to have larger pores on the order of 50 to 1000 nm (Macropores), whereas pores that originated in diagenetic clay minerals were typically smaller than 50 nm, therefore falling in the Mesopore range. Loucks et al. (2012) simplify the pore types by focusing only on the matrix pores, dividing them up into interparticle (interP), intraparticle (intraP) and intraparticle organic matter pores (OM). Interparticle pores consist only of the pores that occur within single particles. Intraparticle pores consist of pores between particles. In general the intraP pores are larger than interP pores. The organic matter pores (OM) consist

Solid Earth Discuss., doi:10.5194/se-2016-38, 2016
Manuscript under review for journal Solid Earth
Published: 16 March 2016
© Author(s) 2016. CC-BY 3.0 License.



within the organic matter and in part reflect the maturity state of the organic matter. In this study we were able to separate the pores in the organic matter, from the other pores. The other pores consist of mainly matrix pores and fracture or desipores, which we separate by size. The smallest pores with a radius of less than 100 nm (=200 nm diameter) as consisting as mainly interP pores, while the larger pores are dominated by intraP pores.

Pores in shales are very difficult to model because of their large size range distribution as mentioned above. The smallest pores are in nm range especially in clay minerals and organics and the largest pores in the mm range that is 6 orders of magnitude. For FIB-SEM the pores that can in general be visualized in our study starting at 25nm and end in nm range, representing almost two orders of magnitude. A question that frequently arises is how representative are FIB-SEM measurements regarding the properties of the whole material, since only a very small volume is investigated. Several works made an attempt to determine the size of representative volume elements (RVE). Based on the statistical approach of Kanit et al. (2003) the cube lengths of RVEs were determined for Opalinus clay (Keller et al., 2013) and for Boom Clay (Hemes et al., 2015). Keller et al. (2013) have shown that the relative error for porosity is about 40-50 % if only one FIB volume of 10^3 μm^3 is investigated. Extrapolations of RVE lengths suggest that the relative error will decrease to <10 % if the cube length of the investigated volume is in the hundreds of microns or if the number of realizations is increased. Hemes et al. (2015) agree with Keller et al.'s (2013) findings and further conclude that FIB analyses alone are not capable of covering spatial inhomogeneities and that a combination of methods (FIB, BIB, µCT) should be favored to characterize 3D porosities. However, the approach of Kanit et al. (2003) is in general rather used to downscale a given volume than to upscale from a smaller one. The biggest problem with upscaling is that the porosity is strongly depended on mineralogy as suggested by Schieber (2011). FIB volumes often do not cover the whole mineralogy or over represent single phases based on their large grain sizes. One could imagine a µm sized pyrite framboid, a very common trace component of shales that lies within a typical 10^3 μm^3 FIB volume. It would not only overestimate the pyrite content but also the porosity, since it has a high internal porosity as shown by Schieber (2011). Quantifying the mineralogy in SE and BSE image volumes is challenging since grey scale values for silicates are often very similar. Nonetheless, results could be used in an "elementary building blocks" model as proposed by Desbois et al. (in press). A first step towards this idea was made in this study where we differentiated between pore space and organics and where we used this data to predict permeabilities and flow velocities.

2 Methods / Results

2.1 Image acquisition and processing

The FIB-SEM analyses were performed on a Zeiss Auriga with EDX and FE-Cathode. The tilt corrected BSE and SE images were collected with a current of 1.5 kV to reduce charging and improve resolution. For slicing 500 pA has been used, resulting in 25 nm thick slices. Voxel size is dependent on the slice thicknesses as well as magnification. The resulting voxel size was 40*40*25 nm for HAD and 56*56*25 nm for WIC. In the following x- and y-directions are referred to as the horizontal and vertical image directions. Z is equal to the direction of the slicing. Before the slice and view, we sputtered the

Solid Earth Discuss., doi:10.5194/se-2016-38, 2016
Manuscript under review for journal Solid Earth
Published: 16 March 2016
© Author(s) 2016. CC-BY 3.0 License.



sample with Pd to minimize charging and improve the imaging of the slices. The result of the slice and view were 400 SE and BSE images. After the image collection the slices were aligned, the images filtered, the porespace and organics binarized and qualitatively and quantitatively analyzed, for which the Avizo-Fire 9.0 and GeoDict software was used. Images were filtered in Avizo by applying a shading correction filter, a FFT filter to remove vertical stripes and a Non-Local Means filter in 2D mode to remove noise. 2D was chosen over 3D because the generated FIB volume is a stack of 2D images rather than real 3D data. The Non-Local Means was preferred because it removes noise without blurring the contrasts between the organics and pore space and without decreasing the resolution of the pores and the organics. Therefore it is possible to clearly distinguish between these phases and the matrix (Figure 1). At times it is difficult to differentiate between pore and organic based on grey scale values especially for small phases within the mineral matrix as can be seen in Figure 1. Effects of these difficulties in distinguishing between these two phases are being discussed later.

After the binarization we resampled the pore space creating cubic voxels (25 nm), essential when determining orientations of the pores. The resulting volume was slightly cropped to meet GeoDict modelling requirements. The pore space was separated into individual pore clusters with quite extensive pore networks (Figure 2). For this study we considered a cluster (organic respectively) if the labelled object is connected by voxels which share a face, edge or vertex. Vertex connection was allowed since GeoDict can model transport along these links. The separated pores/clusters were tested for axis connectivity. The porosity is described by its individual volume, open and closed porosity (Table 1), continuous pore size distribution (Figure 5) and pore path orientation (Figure 7).

2.2 Porosity and pore size distribution

After processing the pore space was visually analysed. In Figure 2 the 10 largest pore clusters of the two samples reveal strong similarities. In both samples the pore clusters run mainly through the mineral matrix but are in places in contact with the smaller organic particles. All of these clusters are made up of a complex pore network as shown in Figure 3 with flow being the fastest in the pore necks.

The total porosity obtained from FIB-SEM is very low compared to other methods as shown by Kaufhold et al. (in press) (WIC – FIB: 1.5%, MIP: 11,9 %; HAD – FIB: 2.4 %, MIP: 8,0 %). Similar results were reported by Keller et al. (2011) for Opalinus clay who obtained a FIB porosity of 1-2 % compared to a N2 porosity of 10-12 %.

The test for axis connectivity showed that no connection of pores exists between the different axes. Open and closed porosity analysis (Table 1) revealed that for HAD only 1/3 of the total pore space has a connection to the borders of the volume (1/6 for WIC). This shows that most of the pores lie isolated within matrix or the organics.

Münch & Holzer (2008) showed that the continuous pore size distribution determined from FIB-SEM can be compared with other analytical methods quantifying the pore size distribution (MIP, N2, CO2). However, the absolute porosity cannot be determined by FIB-SEM due to the limitations of resolution and investigated volume. Nonetheless, results show good agreement of FIB-SEM pore size distributions of this study and MIP performed on the same samples by Kaufhold et al. (in press) when only the range of the overlapping pore radii of both methods is compared (Figure 5). Comparing the MIP data

Solid Earth Discuss., doi:10.5194/se-2016-38, 2016
Manuscript under review for journal Solid Earth
Published: 16 March 2016
© Author(s) 2016. CC-BY 3.0 License.



with the FIB-SEM results show that the FIB-SEM of the WIC sample under estimates pore radii larger than 150 nm by about 0.2 % total porosity compared to MIP. Sample HAD on the other hand over estimates the pore radii smaller than 150 nm compared to MIP measurements. As shown in Figure 1 the 0.9 % more porosity of sample HAD is mainly composed of pores smaller than 100 nm, indicating an increase in small pores with higher thermal maturity.

2.3 Organics

It is not always easy to distinguish in SEM images the organics from the pore space. We used the SE images to separate the two based on the gray scale. Figure 1 shows that the gray scale of organics and pore space are close to each other, but using correct contrast conditions they can be differentiated. The organics for both samples show connectivity between the different axes. The total volume of the organics in the WIC sample is 21.8vol% and in the HAD sample is 12.3vol%. Using a density of 1.25g/cm^3 the TOC in wt% was calculated. This resulted in 11.8 wt% TOC in WIC and 6.1% in HAD. This compares fairly well with the TOC results from Kaufhold et al. (2015) (WIC 8.5 wt% TOC & HAD 5.2 wt%).

Visually it can be seen that with increasing maturity the pore space (>25nm) in the organics increase. The organics in WIC have very few pores while the HAD organics are filled with pores. We binarized the largest organic particle together with its pore space in HAD (Figure 4). The results were that the organic particle contained an internal pore space of 5.5%. The binarized pores contain only a small network of pores and are not interconnected with the surrounding mineral matrix, suggesting that they may have been gas filled when they were sampled.

2.4 Permeability calculations

The pores for both samples do not show any connectivity (permeability = 0) between the different sides. The next assumption we made was that, the organics had an own extremely low permeability of 1e-22 m^2 itself (similar to Monteiro et al., (2012) and corresponding to a diameter of 3.2 nm, after tube flow model) and assign this number to the organic phase in the binarized domain to apply a coupled free air and porous media flow. Doing this, a connected porous media was build up and the organics with the small pores below the FIB detection resolution limit contributed to the pressure drop and flux. This allowed us to perform permeability calculations using GeoDict. The permeability tensors for both pores and organics were calculated for binarized images (resolution 25 nm per voxel, dimension of computational domain is 768x768x384 respectively 768x512x384) with as special Navier Stokes-Brinkman LIR solver for coupled free and porous media flow and implemented in the GeoDict software (Iliev and Laptev, 2004; Wiegmann, 2007). To determine a tensor of permeability, it is necessary applying each side of the domain in x,y,z direction with an pressure gradient separately and simulate the flux through the sample. As fluid, we use air with a temperature of 293.15 K, a density of 1.204 kg/m3 and a dynamic viscosity of 1.834E-5 kg/(m·s). The boundary conditions were pressure gradient in flow directions as constant boundaries and all other domain sides were defined as symmetric (mirrored over sides) with periodic boundary conditions (Khan et al., 2012). These setups give numerically accurate flow simulations in low and heterogeneous porous structures. Simulations will stop, if the system reaches steady state and the flux will become constant over time meaning that numerical accuracy of 1e-4 m² residual

Solid Earth Discuss., doi:10.5194/se-2016-38, 2016
Manuscript under review for journal Solid Earth
Published: 16 March 2016
© Author(s) 2016. CC-BY 3.0 License.



permeability is reached. Figure 6b shows the resulting pressure field for one side case after numerical convergence. The resulting pressure and velocity fields are shown in Figure 3 and Figure 6. If we assume this organic permeability, the total permeability increases by a factor of up to 10 in sample HAD and by a factor of up to 100 for WIC if compared to the permeability of organic matter (Table 1).

These are in a range of experimental determined permeabilities in clay rocks (Javadpour, 2007 & Zhang, 2016). Permeabilities show spatial anisotropies. For the HAD sample, the lowest permeability was observed in the y-direction (6.81e-22 m²). WIC showed lowest permeability in y and z (1.16e-21 and 1.37e-21 m²). The resulting average velocities for air flow at 100000 Pa show a similar anisotropy, where lowest velocities are observed in x and y for HAD (2.8e-7 and 2.9e-7 m/s) and in y for WIC (3.3e-7 m/s). Velocities for the water flow are two orders of magnitude lower than for air in the y and z direction of both samples and for the x direction of WIC. Only little differences were observed for HAD in x direction.

2.5 Pore path orientation

The spatial distribution of the pore paths was evaluated by analyzing stereographic projections. A skeleton of the binarized pore space was generated by using the *Centerline Tree* module of Avizo 9.0 (Tube parameter: *slope* = 3:5; *zeroV al* = 4). It is based on the TEASAR algorithm (Sato et al., 2000) which generates tree-like vector based skeletons that do not allow circles. Dip and plunge of each vector were plotted using *Stereonet* software of Cardozo and Allmendinger (2013). Orientation of a vector represents the orientation of the pore path. It does not take into account how long or skewed the path itself is. Only pores larger than 200 voxels were analyzed in order to obtain reliable orientations. Equal area projections in combination with 1 % net area contouring (interval: 1 %) were used for a better visualization.

Results are shown in Figure 7**.** It becomes apparent that pore paths in sample HAD are oriented homogenously along the bedding plane which is equal to the x-z plane. In contrast sample WIC shows a strong preferred orientation that differs from the x-z plane, what indicates that the slicing with the FIB was not performed perpendicular to the bedding plane

3. Discussion

3.1 Porosity

Porosity using FIB-SEM can be described either as pore clusters or through continuous pore size distribution (PSD). PSD describes best the pore geometry and therefore hydrodynamic properties in shales. The thin throats within the pore clusters are what control its hydrodynamic properties (Figure 3). The typical range of pores in these organic rich shales are between 25 and 300 nm similar to the Opalinus clay (5-300 nm) from Keller et al. (2013). The PSD trends of HAD and WIC are almost identical between 300 and 100 nm while for the mature sample HAD for pores with radii <100 nm increase by 0.9% compared with WIC. This supports the argument that during maturation small pores formed. What complicates this issue, as already mentioned, is that many pores are out of the range of the resolution and that a fraction of small pores within the mineral matrix is misinterpreted as organic (Figure 1). Therefore, the increase in the volume generated by radii <100 nm in

Solid Earth Discuss., doi:10.5194/se-2016-38, 2016
Manuscript under review for journal Solid Earth
Published: 16 March 2016
© Author(s) 2016. CC-BY 3.0 License.



the PSD should be much bigger. This would result in higher total porosity values as well. The 0.9 % more total porosity of sample HAD compared to WIC is made of pores <100 nm. This is caused by small pores within organics which are easier to identify as pores than those within in mineral matrix and HAD contains small pores within in the organic, which is not the case in the WIC sample. The increase in thermal maturity only leads to an increase in porosity but not in connectivity, because the new formed pores are isolated, closed pores within the organics.

Although we were able to show that the pores align along the bedding plane, no connectivity between the axes was observed in both samples. Similar results have been reported by Keller et al. (2013) who found that the connectivity of shales is highest along the bedding plane and decreases with increasing sample length. Further they conclude that the connectivity depends on the porosity of the investigated volume and that a local porosity between at least 6 and 10 % is needed to realize percolation paths along the bedding plane. These findings are supported by Hemes et al. (2015) who found that at a total porosity of about 18 % almost 87 % the pore space contribute to the axis connectivity. In our work we observed that at porosities of about 2 % connected pore clusters only exist at the scale of a few µm. When considering the misinterpretation of pores as organics we can assume that the real connectivity of pores is much higher, since we have already shown that if we combine pores and organics all axes are connected. Improvements in image resolution could offer valuable clues to solve this problem. However, Kuila et al. (2014) state that in organic-rich shales 10-70 % of the total porosity might not even be detectable with methods like field emission scanning electron microscopy, due to too small pore sizes (<5 nm) within organics and clays.

3.2 Permeability

As shown in Figure 6 **Fehler! Verweisquelle konnte nicht gefunden werden.** the pressure field develops continuously when the size of pores and organics is rather large. Jumps appear when the connectivity is limited by thin throats or is not given at all (Fig. 5b, WIC bottom right). After analyzing the pressure field for all directions it becomes obvious that the pathways through the material are restricted by those throats throughout the material. The velocity fields illustrate this as well. Flow of air and water only appears within parts of the pore. Figure 3 shows a close-up of the skeleton of single pore cluster in combination with the velocity field. By comparing both we found that the highest velocities are reached within throats between areas where the pore is rather thick and where velocities are comparatively low.

Permeability and average velocity calculations for HAD correspond very well to the analysis of the pore path orientation. As shown in Figure 7 the bedding is horizontal and parallel to the x-z-plane. Permeability and the velocity for water are highest along the bedding which is in good agreement with the results of Bhandari et al. (2014) who have shown an anisotropic behavior of the gas permeability for the Barnett Shale, a similar shale in mineralogical composition, thermal maturity and TOC content. They measured a permeability of 2.3e-21 m² perpendicular to the bedding and 9.5e-20 m² parallel to the bedding, both similar to our calculations.

Solid Earth Discuss., doi:10.5194/se-2016-38, 2016
Manuscript under review for journal Solid Earth
Published: 16 March 2016
© Author(s) 2016. CC-BY 3.0 License.



Permeabilities of HAD and WIC differ by one order of magnitude. This is likely caused by the higher organic contents in sample WIC (22% compared to 12% for HAD). Larger amounts of organics lead to larger amounts of open porosity that participates in transport processes.

The approach to include the organics into the simulations with a permeability of 1e-22 m² resulted in permeability values that show good agreement with experimental data of other researchers. A series of permeability measurements on 152 samples of 9 potential shale gas formations performed by Javadpour et al. (2007) showed an average permeability of 54 nD (5,3e-20 m²) meaning that the results of the simulations performed in this work fit well into this range. Similar values are reported by Zhang (2016).

With increasing thermal maturity the amount of kerogen content decreases by 7% and resolvable nm-sized pores develop within the remaining organic matter. Although more pores should enhance flow properties the opposite is the case. However decrease in OM content (-7 %) is too large to compensate for the increase in porosity (+0.9 %). As a result of the lower organic content is that the permeability decreases. This highlights the important role of kerogen in the transport of gas through shale since it acts as a connector of else closed, isolated pores.

4. Conclusions

1. The pore space increases inside in the organic matter during maturation. These newly developed pores are likely to have been filled with gas due to their small size and the lack of connectedness to the mineral matrix. The volume of pores (5.5%) in the organics that have been developed compare well with the 2D observations made by Curtis et al 2012, who quantified the pore space with increasing maturity and found for the most part that the pore space increased within the organics during maturation. This suggests that hydrocarbons are likely to still be in place and in the case of gas may be activated.

2. The continuous pore size distribution (both FIB-SEM and MIP) of the total studied volume shows that the mature sample contains much smaller pores indicating that new small pore space was developed during the maturation.

3. The largest pore clusters have not changed significantly during maturation, suggesting the organics have changed but the pores within the mineral matrix have not. The total FIB-SEM porosity of 2% is too low to have developed a connectivity in the 10s of micrometer range. Therefor the pore space in the organics and clay minerals that cannot be seen with FIB-SEM provide the connectivity of the migrating fluids. The clay mineralogy, especially the illite smectite did not significantly change during the maturation, suggesting little diagenetic alteration of the pore clusters.

4. The modelled total permeabilities, assuming a permeability of 1e-22 m^2 for the organic matter, compare well to values reported in literature. The observed anisotropy is in the same order of magnitude as reported by Bhandari et al. (2014). Further, the decrease in OM content, with higher thermal maturity, effects the flow properties more than the increase in porosity.

© Author(s) 2016. CC-BY 3.0 License.



References

Bernard, S., and Horsfield, B., and Schulz, H.M., and Wirth, R., and Schreiber, A., and Sherwood, N.: Geochemical evolution of organic-rich shales with increasing thermal maturity: A STXM and TEM study of Posidonia Shale (Lower Toarcian, northern Germany), Mar. Pet. Geol., 31, 70-89, doi:10.1016/j.marpetgeo.2011.05.010, 2011.

Bhandari, A.R., and Flemings, P.B., and Polito, P.J., and Cronin, M.B., and Bryant, S.L.: Anisotropy and stress dependence of permeability in the Barnett Shale, Transp. Porous Med, doi:10.1007/s11242-015-0482-0, 2015.

Cardozo, N., and Allmendinger, R.W.: Spherical projections with OSXSteronet, Computers and Geosciences, 51, 193-205, doi:10.1016/j.cageo.2012.07.021, 2013.

Chalmers, G.R., and Bustin, R.M., and Power, I.M.: Characterization of gas shale pore systems by porosimetry, porosimetry, surface area and field emission scanning electron microscopy/transmission electron microscopy image analyses: Examples from the Barnett, Woodford, Haynesville, Marcellus and Doig units, APPG Bulletin, 96, 1099-1119, doi:10.1306/10171111052, 2012.

Curtis, M.E., and Cardott, B.J., and Sondergeld, C.H., and Rai, C.S.: Development of organic porosity in the Woodford Shale with increasing thermal maturity, Int. J. Coal Geol., 103, 26-31, doi: 10.1016/j.coal.2012.08.004, 2012.

Desbois, G., and Urai, J.L., and Hemes, S., and Schröppel, B., and Schwarz, J.-O., and Mac, M., and Weiel, D.: Multi-scale analysis of porosity in diagenetically altered reservoir sandstone from the Permian Rotliegend (Germany), Journal of Petroleum Science and Engineering, doi:10.1016/j.petrol.2016.01.019, (in press).

Hemes, S., and Desbois, G., and Urai, J.L., and Schröppel, B., Schwarz, J.-O.: Mutli-scale characterization of porosity in Boom Clay (HADES-level, Mol, Belgium) using a combination of X-ray μ-CT, 2D BIB-SEM and FIB-SEM tomography, Microporous and Mesoporous Materials, 208, 1-20, doi:10.1016/j.micromeso.2015.01.022, 2015.

Horsfield, B., and Littke, R., and Mann, U., and Bernard, S., and Vue, T.A., and di Primio, R., and Schulz, H.M.: Shale Gas in Posidonia Shale, Hils Area, Germany, Search and Discovery Article #110126, 2010.

Iliev, O., and Laptev, V.: On numerical simulation of flow through oil filters, Comput Visual Sci, 6, 139-146, doi:10.1007/s00791-003-0118-8, 2004.

© Author(s) 2016. CC-BY 3.0 License.



Javadpour, F., and Fisher, D., and Unsworth, M.: Nanoscale Gas Flow in Shale Gas Sediments, Journal of Canadian Petroleum Technology, 46, 55-61, doi:10.2118/07-10-06, 2007.

Kanit, T., and Forest, S., and Galliet, I., and Mounoury, V., and Jeulin, D.: Determination of the size of the representative volume element for random composites: statistical and numerical approach, Int. J. of Solids and structures, 40, 3647-3679, doi:10.1016/20020-7683(03)00143-4, 2003.

Kaufhold, S., and Grathoff, G.H., and Halisch, M., and Plötze, M., and Kus, J., and Ufer, K., and Dohrmann, R., and Ladage, S., and Ostertag-Henning, C.: Comparison of methods for the determination of the pore system of a potential German gas shale, Clays and Clay Minerals, (in press).

Keller, L.M., and Holzer, L., and Schuetz, P., and Gasser, P.: Pore space relevant for gas permeability in Opalinus clay: Statistical analysis of homogeneity, percolation, and representative volume element. Journal of Geophysical Research: Solid Earth, 118, 2799-2812, doi:10.1002/jgrb.50228, 2013.

Keller, L.M., and Holzer, L., and Wepf, R., and Gasser, P.: 3D geometry and topology of pore pathways in Opalinus clay: Implications for mass transport, Applied Clay Science, 52, 85-95, doi:10.1016/j.clay.2011.02.033, 2011.

Khan, F., Enzmann, F., Kersten, M., Wiegmann, A., and Steiner, K.: 3D simulation of the permeability tensor in a soil aggregate on basis of nanotomographic imaging and LBE solver, J Soils Sediments, 12, 86-96, doi:10.1007/s11368-011-0435-3, 2012.

Klaver, J., and Desboi, G., and Urai, J.L., and Littke, R.: BIB-SEM study of pore space morphology in early mature Posidonia Shale from the Hils area, Germany, Int. J. Coal Geol., 103, 12-25, doi:10.1016/j.coal.2012.06.012, 2012.

Loucks, R.G., and Reed, R.M., and Ruppel, S.C., and Hammes, U.: Spectrum of pore types and networks in mudrocks and a descriptive classification for matrix-related mudrock pores., APPG Bulletin, 96, 1071-1098, doi:10.1306/08171111061, 2011.

Monteiro, P. J. M., and Rycroft, C.H., and Barrenblatt, G.I.: A mathematical model of fluid and gas flow in nanoporous media. PNAS, 109, 20309-20313, doi:10.1073/pnas.1219009109, 2012.

Muench, B., and Holzer, L.: Contradicting geometrical concepts in pore size analysis attained with electron microscopy and mercury intrusion, Journal of the Amercian Ceramic Society, 91, 4059-4067, doi:10.111/j.1551-2916.2008.02736.x, 2008.

© Author(s) 2016. CC-BY 3.0 License.



Rouquerol, J., and Avnir, D., and Fairbridge, C.W., and Everett, D.H., and Haynes, J.M., and Pernicone, J.M., and Ramsay, J.D.F., and Sing, W., and Unger, K.K.: Recommendations for the characterization of porous solids, Pure & Appl. Chem., 66, 1739-1758, doi:10.1351/pac199466081739, 1994.

Sato, M., and Bitter, I., and Bender, M., and Kaufman, A.E., and Nakajima, M.: TEASAR: Tree-Structure Extraction Algorithm for Accurate and Robust Skeletons, Pacific Conference on Computer Graphics and Applications, 8, 281-449, doi:10.1109/PCCGA.2000.883951, 2000.

Schieber, J.: Shale microfabrics and pore development – an overview with emphasis on the importance of depositional processes, Gas Shale of the Horn River Basin (Eds: Leckie, D.A. and Barclay, J.E.), 115-119, 2011.

Schlosser, J., and Grathoff, G.H., and Ostertag-Henning, C., and Kaufhold, S., and Warr, L.N.: Mineralogical changes in organic-rich Posidonia Shales during burial and experimental maturation, Int. J. Coal Geol., doi:10.1016/j.coal.2015.07.008, (in press).

Wiegmann, A.: Computation of the permeability of porous material from their microstructure by FFF-Stokes. Berichte des Fraunhofer ITWM 129, 2007.

Zhang,C.L: The stress-strain-permability behaviour of clay rock during damage and recompaction, J Rock Mech and Geotechn Eng., 8,1,16-26, 2016.

Solid Earth Discuss., doi:10.5194/se-2016-38, 2016
Manuscript under review for journal Solid Earth
Published: 16 March 2016
© Author(s) 2016. CC-BY 3.0 License.

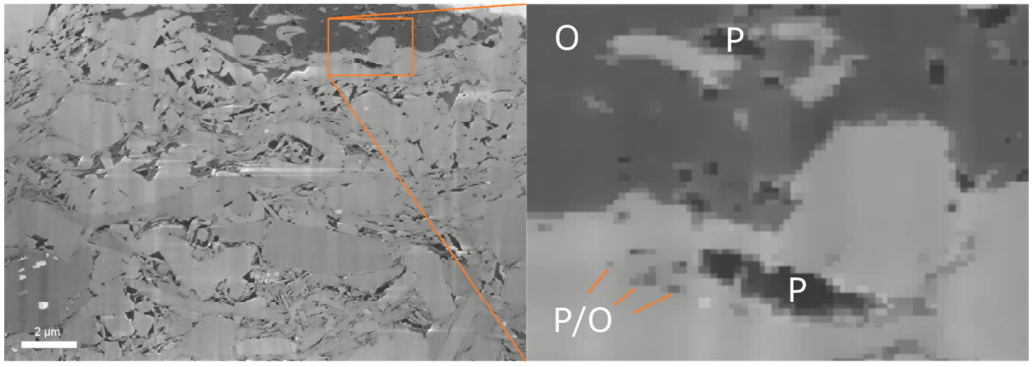

Figure 1: Image of filtered slice on the left and enlarged red box on the right. Black is the pore space, dark gray organics. On the right enlarged red box, the pore space is black (pixel size in this image is 40 nm). In 2 D the pores are not connected but in 3D some of the pores are connected, grouped into clusters.

5

Solid Earth Discuss., doi:10.5194/se-2016-38, 2016
Manuscript under review for journal Solid Earth
Published: 16 March 2016
© Author(s) 2016. CC-BY 3.0 License.

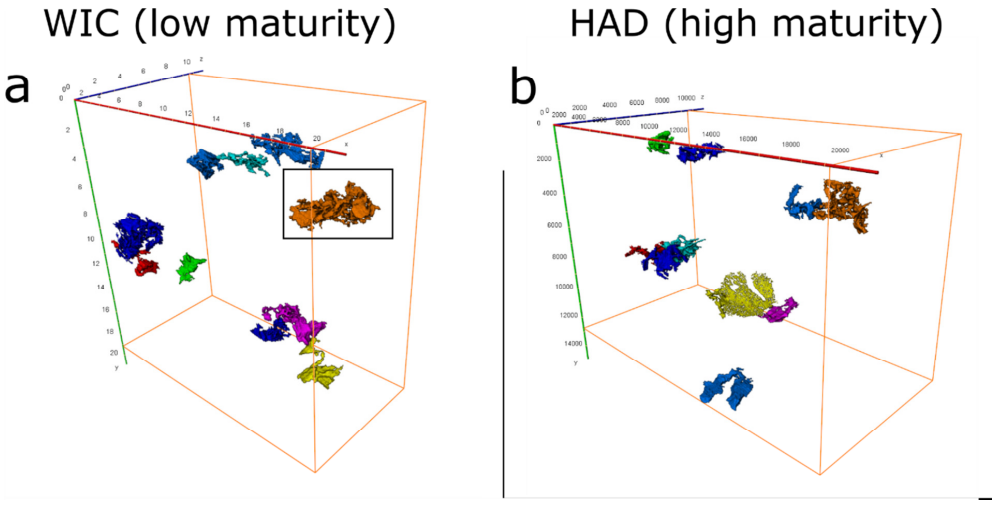

Figure 2: 10 biggest pore clusters of sample WIC and HAD. No big differences were observed in size, pore size distribution and connectivity for the two samples.

Solid Earth Discuss., doi:10.5194/se-2016-38, 2016
Manuscript under review for journal Solid Earth
Published: 16 March 2016
© Author(s) 2016. CC-BY 3.0 License.

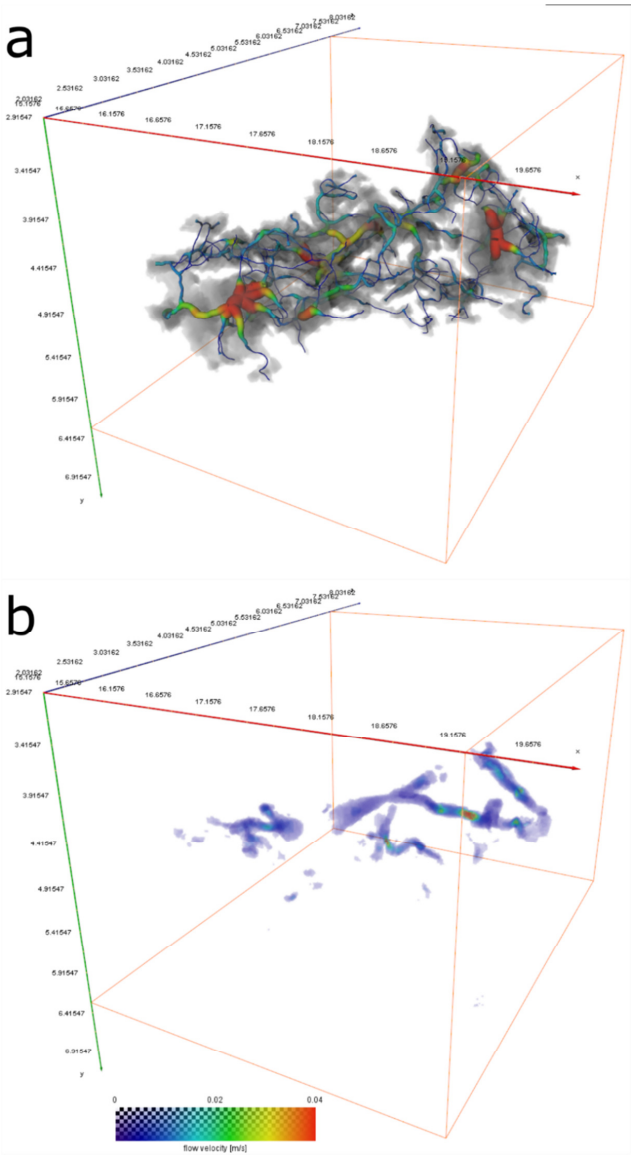

Figure 3: Orange pore cluster from sample WIC (see Figure 2 for location). A. skeleton transformation of the cluster. Colors represent relative thickness of the pore at that position (blue – thin, red –thick). B. Velocity field of the GeoDict calculations in z-direction for air as flowing phase. It is shown that only little of the total pore cluster participates in phase flow. Velocities increase in regions that form thin throats.

Solid Earth Discuss., doi:10.5194/se-2016-38, 2016
Manuscript under review for journal Solid Earth
Published: 16 March 2016
© Author(s) 2016. CC-BY 3.0 License.

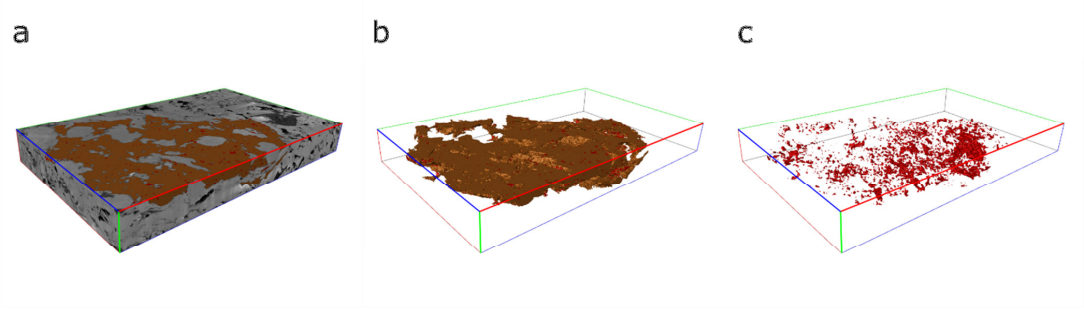

Figure 4: The analysis of the biggest organic cluster of sample HAD revealed that organics contain small unconnected pores. A total porosity of 5.5 % was observed within the cluster. These pores are formed during the thermal maturation of the shale.

Solid Earth Discuss., doi:10.5194/se-2016-38, 2016
Manuscript under review for journal Solid Earth
Published: 16 March 2016
© Author(s) 2016. CC-BY 3.0 License.

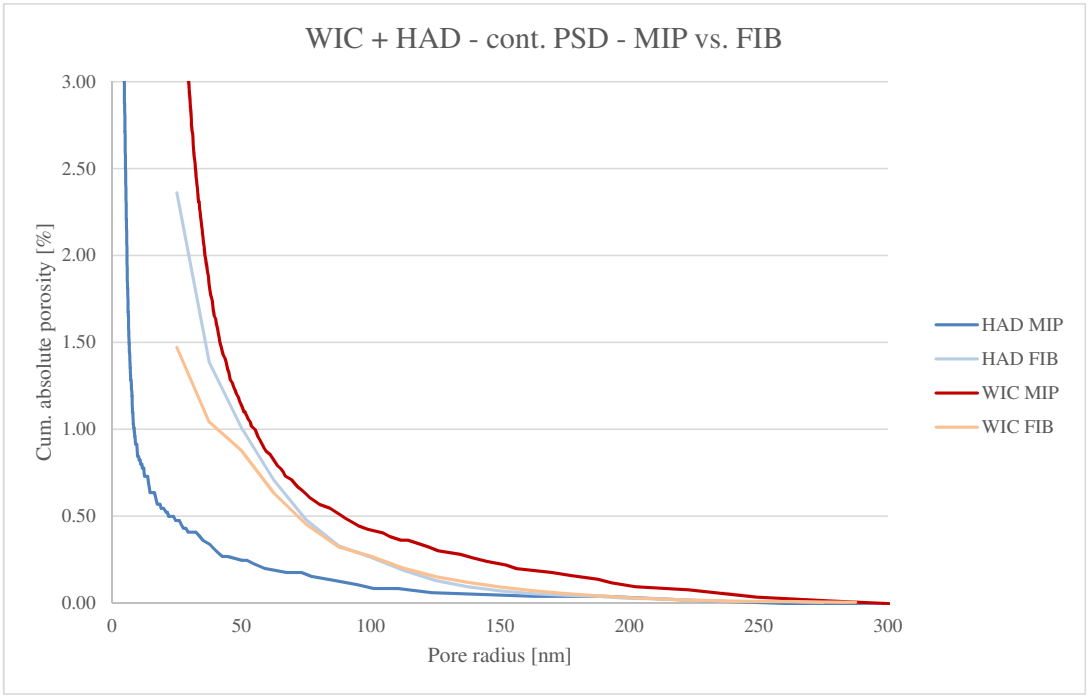

Figure 5: Plot of continuous pore size distribution (FIB), compared to Mercury intrusion porosimetry (MIP) data from Kaufhold et al. (in press).

Solid Earth Discuss., doi:10.5194/se-2016-38, 2016
Manuscript under review for journal Solid Earth
Published: 16 March 2016
© Author(s) 2016. CC-BY 3.0 License.

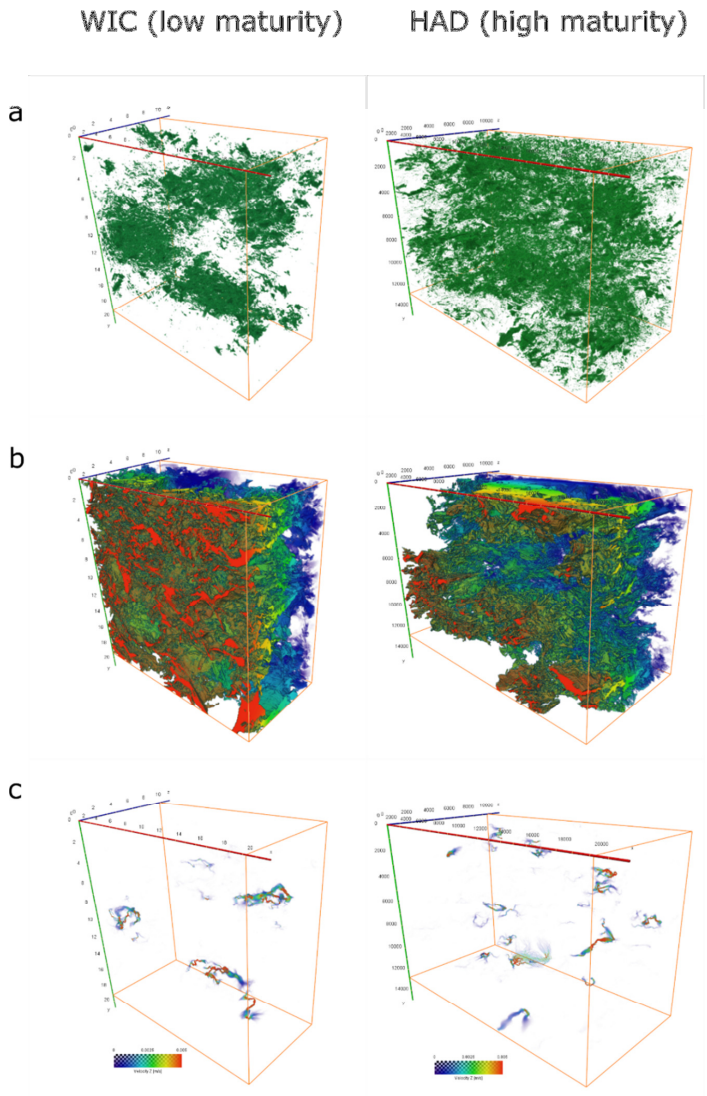

Figure 6: A. Binarized pore volume. It was observed that small pores were mainly formed within organics and the clay mineral matrix. B. Pressure fields in z-direction resulting from GeoDict calculations. Jumps within the field were observed when throats become very thin or when a physical connectivity of the pores was not given. Regions where organics dominate show a continuous gradient. C. Velocity field in z-direction. Flow only takes place in regions that are dominate by pores. For a closeup the flow field in a single pore cluster see Figure 3.

Solid Earth Discuss., doi:10.5194/se-2016-38, 2016
Manuscript under review for journal Solid Earth
Published: 16 March 2016
© Author(s) 2016. CC-BY 3.0 License.

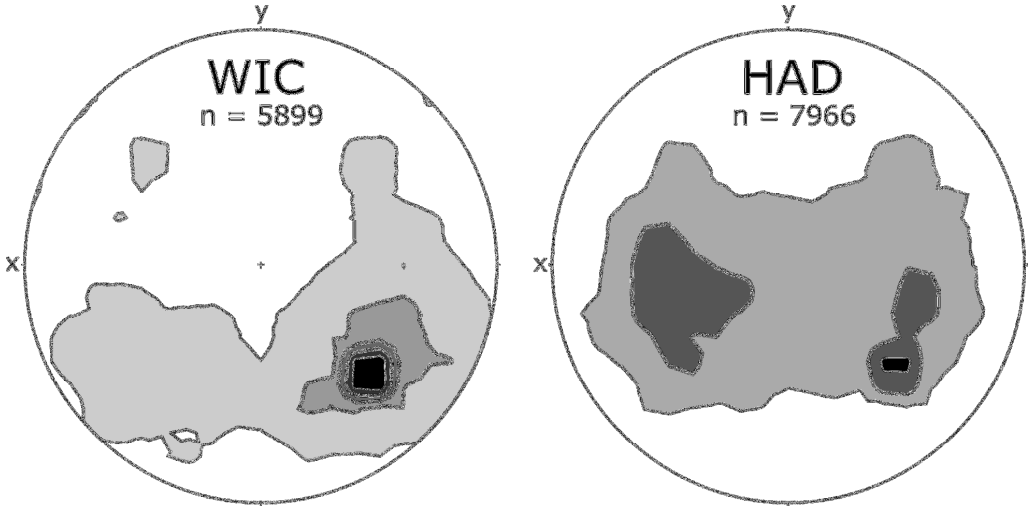

Figure 7: Pore path orientation of sample WIC and HAD using 1% net area contouring with an interval of 1%. WIC shows a strong preferred orientation and a dip of 45°, which indicates a deviation between x-z-plane and bedding plane. Pore paths of HAD show a homogeneous distribution along the bedding plane.

Solid Earth Discuss., doi:10.5194/se-2016-38, 2016
Manuscript under review for journal Solid Earth
Published: 16 March 2016
© Author(s) 2016. CC-BY 3.0 License.



Solid Earth Discussions
Open Access
EGU

Table 1: Results of GeoDict permeability simulations and porosity analyses. Note that Open and Closed porosity calculations were performed on the binarized volumes including cluster sizes smaller than 10 voxels so summarized porosities may differ. (k – permeability in x,y,z; v – velocities for air and water flow in x, y, z)

	WIC	**HAD**
k_x **[m²]**	1.19E-20	9.91E-22
k_y **[m²]**	1.16E-21	6.81E-22
k_z **[m²]**	1.37E-21	1.82E-21
$V_{air\text{-}x}$ **[m/s]**	3.39E-06	2.81E-07
$V_{air\text{-}y}$ **[m/s]**	3.29E-07	2.90E-07
V_{air_z} **[m/s]**	7.76E-07	1.04E-06
$V_{water\text{-}x}$ **[m/s]**	6.22E-08	5.16E-07
$V_{water\text{-}y}$ **[m/s]**	6.03E-09	5.32E-09
$V_{water\text{-}z}$ **[m/s]**	1.42E-08	1.90E-08
Total porosity [vol%]	1.47	2.61
Open porosity [vol%]	0.23	0.58
Closed porosity [vol%]	1.23	1.77
Total organic content [vol%]	21.92	14.71
Open organic content [vol%]	21.64	13.94
Closed organic content [vol%]	0.28	0.77